

Chapter 1

UXO SIGNAL MULTI SENSOR DETECTION AND ESTIMATION *

Chr. Kabakchiev¹, V. Behar², B. Vassileva², D. Angelova², K. Aleksiev²,
V. Kyovtorov³, I. Garvanov³, L. Doukovska³, and P. Daskalov⁴

Abstract

In this chapter, the original advanced algorithms for stepped-frequency GPR imaging are considered. In stepped-frequency GPR, the range profile formation is carried out by reconstruction of a wideband chirp by combining a set of stepped-frequency chirp signals in the time domain. Using the Modelsim simulator, it is shown that the processor VIRTEX II Pro is suitable for implementation of this algorithm. A simple convolution algorithm for simulation of stepped-frequency GPR images from multi-layered subsurface media is described. Different approaches and algorithms for the basic GPR signal and image processing are also considered in this chapter. These algorithms are used for improving the image quality of underground objects, e.g. pipes. It is shown that applying different filters (CFAR, Hough, Kalman, Particle) to GPR image processing is a good decision in the sense of estimation accuracy, probability of target detection and false alarm.

1 Faculty of Mathematics and Informatics, Sofia University

“James Bourchier” Str., 5, 1164 Sofia, Bulgaria

e-mail: ckabakchiev@fmi.uni-sofia.bg, ckabakchiev@yahoo.com

2 Institute for Parallel Processing, Bulgarian Academy of Sciences

“Acad. G. Bonchev” Str., bl. 25-A, 1113 Sofia, Bulgaria

e-mail: behar@bas.bg

3 Institute of Information Technologies, Bulgarian Academy of Sciences

“Acad G. Bonchev” Str., Bl. 2, 1113 Sofia, Bulgaria

e-mail: vladimir.kyovtorov@gmail.com, igarvanov@yahoo.com, l.doukovska@mail.bg

4 Multiprocessor Systems Ltd.

Shipchensky prohod Blvd., 63, 1574 Sofia, Bulgaria

e-mail: Daskalov@mps.bg

* This work was financially supported by the Bulgarian National Science Fund (grants MI-1506/2005 and BG051PO001/07/3.3-02-7/08), the National Innovation Fund (grant IF-02-85/2005) with MPS Ltd. Project “Digital Ground Penetrating Radar” and IIT 010089/2007.

1.1 Introduction (UXO Signals and a Multi Sensor Approach)

Ground penetrating radar (GPR) is a well-known method of subsurface exploration, which becomes extremely important for many environmental applications such as unexploded ordnance (UXO) detection and geophysical implementation [8]. It is well-known that most commercial GPR systems are ultra-wideband pulse radars, in which range resolution is determined by the bandwidth of the transmitted pulse. In these GPR, high range resolution is achieved by transmitting very short pulses (or frequency-modulated pulses) to obtain the required bandwidth. The frequency-stepped processing method is a technique developed to overcome the power bandwidth limitations of pulse radars.

In this chapter, GPR range profile formation is carried out by reconstruction of a wideband chirp by combining a set of stepped-frequency chirp signals in the time domain. In order to optimize the parameters of the stepped-frequency algorithm, a simple convolution-based algorithm for simulation of echoes from multi-layered subsurface media has been developed. As a result, a simple algorithm for simulation of frequency-stepped GPR images of multi-layered media has been developed for parameter optimization of the basic GPR signal and image processing [3, 5].

Different approaches and algorithms for the basic GPR signal and image processing are considered and studied in order to improve the image quality of underground objects and enable a recognition of objects and estimation of their parameters. The results of the study described in [1, 2, 3, 4, 5, 6, 9, 10] show that different approaches and algorithms for signal and image processing generally lead to similar results. However, in different situations, there can be alternatives. The results described here are obtained in cooperation with MPS Ltd., the Institute of Information Technologies (IIT-BAS) and the Institute for Parallel Processing (IPP-BAS), within the project “Digital Ground Penetrating Radar” financially supported by the National Innovation Fund (IF-02-85/2005-2007).

According to [8], underground objects of interest (e.g. pipes) are very similar to unexploded ordnance (UXO). Therefore, our first conclusion is that algorithms developed for GPR imaging and also for simulation of GPR images can be successfully used in a system for detection of unexploded ordnance (UXO).

Our second conclusion is that the multi-sensor unexploded ordnance detection system (MUDS) approach, usually leading to image improvement, and the parameter estimation of unexploded ordnance (UXO) by using different types of sensors can also be successfully applied to the same GPR sensors with different algorithms for signal and image processing.

1.2 Stepped-Frequency GPR imaging

The novelty of the results obtained in [5] is that two stepped-frequency methods intended earlier for SAR applications are used for GPR imaging and implemented on the base of RSPs of Analogy Devices. These methods construct a synthetic high-resolution range profile by transmission of a burst of narrowband LFM pulses with frequency bands separated by a fixed step. The first of them constructs the wideband signal in the time domain as a combination of stepped-frequency narrowband chirps. The other method constructs the wide frequency band of a wideband signal as a combination of the frequency bands of stepped-frequency narrowband chirps. In that case, the range resolution of a synthetic range profile produced by GPR depends on the whole frequency range of the transmitted pulses. Starting from the requirements to implement the stepped frequency processing on the base of RSP AD6624 and AD6624A, four optimal parameter sets of the stepped-frequency processing are proposed for its implementation in GPR. The criterion of optimization was the minimal main lobe width and the minimal sidelobe peaks of the output signal in a synthetic range profile of a homogeneous subsurface medium containing a point target. The first variant of optimal parameter sets corresponds to stepped-frequency GPR operating at 4.6 MHz to 38.2 MHz, which generates synthetic range profiles with the range resolution of 1-2 m by transmitting 14 narrowband chirps at each GPR position. The simulation results show that the method of constructing a range profile in the time domain is a more appropriate one because it produces the synthetic range profile with lower noise.

1.2.1 Time-domain processing

The time-domain technique uses a sequence of stepped-frequency narrowband waveforms to produce a high-resolution synthetic range profile. In the time domain, a long wideband chirp is constructed from M narrowband chirps, each of duration T_p , separated in time by a repetition interval T . The central frequencies of narrowband chirps are spaced by step Δf . Since the spectrum of each narrowband chirp is a fraction of a constructed wideband chirp, all transmitted chirps should have the same frequency rate:

$$b_1 = b_2 = \dots = b_M = b = \Delta f / T_p. \quad (1.1)$$

The total bandwidth of a reconstructed wideband pulse is expressed as:

$$\Delta F = f_{max} - f_{min} = \Delta f M. \quad (1.2)$$

The central frequency of a transmitted narrowband chirp changes as:

$$f_{0,m} = f_c + [m - (1 - M)/2]/\Delta f, \text{ where } f_c = (f_{min} + f_{max})/2, m = 1, \dots, M. \quad (1.3)$$

The transmitted pulse belonging to the same burst can be described by:

$$v_{tx}(t, m) = p(t) \exp(j2\pi f_{0,m} t), \text{ where } p(t) = A \text{rect}(t/T_p) \exp(j\pi b t^2). \quad (1.4)$$

The pulse reflected from a point scatterer located at distance d is a time-delayed version of the transmitted pulse, i.e.:

$$v_{rx}(t, m) = v_{tx}(t - \tau, m), m = 1, \dots, M. \quad (1.5)$$

The time delay in (1.5) is $\tau = 2d/V$, and V is the velocity of electromagnetic wave propagation. After quadrature demodulation, the received signal at baseband is given by:

$$v_{bb}(t, m) = v_{rx}(t, m) \exp(-j2\pi f_{0,m} t) = p(t - \tau) \exp(-j2\pi f_{0,m} \tau). \quad (1.6)$$

The construction of a synthetic range profile is performed by the following processing steps:

- *Upsampling.* In order to avoid overlaps in the constructed spectrum, the baseband signals have to be upsampled by a factor of M , where M is the number of transmitted pulses.

- *Frequency shift.* The frequency shift of $v_{bb}(t, m)$ is performed in the time domain as:

$$v'_{bb}(t, m) = v_{bb}(t, m) \exp(j2\pi \delta f_m t), \text{ where } \delta f_m = [m + (1 - M)/2]\Delta f. \quad (1.7)$$

- *Phase correction.* In order to avoid phase discontinuities in the wideband signal, the phase of each narrowband pulse must be corrected by a phase-correcting term, given by:

$$\Phi_m = \exp(j\pi b T_p^2 [m + (1 - M)/2]^2). \quad (1.8)$$

- *Time shift.* Before coherent summing each narrowband pulse is shifted in the time domain by:

$$\delta t_m = [m + (1 - M)/2]/T_p. \quad (1.9)$$

- *Coherent summing.* In the time domain, the wideband pulse $v'(t)$ is formed by coherently summing all the narrowband signals $v'_{bb}(t, m)$:

$$\begin{aligned} v'(t - \tau) &= \sum_{m=0}^{M-1} v'_{bb}(t - \delta t_m, m) \Phi_m = \\ &= A \exp[j\pi b (t - \tau)^2] \sum_{m=0}^{M-1} \text{rect}\left(\frac{t - \tau - \delta t_m}{T_p}\right) = A \exp[j\pi b (t - \tau)^2] \text{rect}\left(\frac{t - \tau}{MT_p}\right). \end{aligned} \quad (1.10)$$

The bandwidth and duration of the wideband chirp $v'(t)$ are equal to $M\Delta f$ and MT_p , respectively.

• *Pulse compression.* The final operation of constructing a synthetic range profile is performed by filtering the constructed wideband pulse (10). The filter impulse response is formed as the time-reversed conjugate of the wideband pulse, which is constructed from the transmitted narrowband pulses. The signal at the compression filter output is given by:

$$r(t) = |FFT^{-1}S(f)V(f)|, S(f) = FFT[s(t)], V(f) = FFT[v'(t - \tau)] \quad (1.11)$$

where $s(t) = conj[v'(t - \tau)]W(t)$ under $\tau = 0$, and $W(t)$ is the weighting function.

1.2.2 Simulation results

The block scheme for formation of a synthetic range profile using the stepped frequency algorithm in the time domain is shown in Figure 1. According to the block scheme, the left channel for signal processing performs echo-signals while the second channel forms the impulse response of a compression filter. The examples of both, the wideband signal and the synthetic range profile, constructed in the time domain by combining 14 narrowband chirps are shown in Figure 2. Comparison analysis of synthetic range profiles

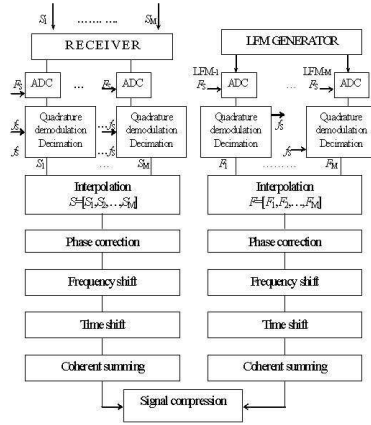


Fig. 1.1 Time-domain method

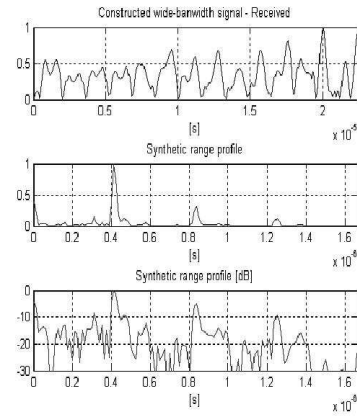


Fig. 1.2 The Synthetic range profile

given in [5] shows that the two stepped-frequency processing methods are of equivalent quality. However, it can be seen that the first method is a more

appropriate one because it produces the synthetic range profile with lower noise.

1.3 Simulation of Stepped-Frequency GPR images

At each transmission of a narrowband pulse, the EM wave radiated from a transmitter antenna travels through the multi-layered media with a velocity that depends on the electrical properties of layers. If the EM wave encounters a boundary between two layers with different electrical properties, a part of the EM energy is reflected or scattered back to the surface, while the rest of the energy continues to travel downward. The radar receiver collects the return signal that contains several returns from various layers of different dielectric properties. There are a variety of methods for simulation of GPR return signals. For a basic first-order simulation, a simple convolution-based modeling technique can be used [6]. More accurate results, taking into account the effects of scattering due to random surfaces and the three dimensional antenna beam pattern can be obtained using advanced methods such as the Finite Difference Time Domain (FDTD) method, at the cost of complexity and computational time.

The novelty of the results obtained in [6] is that a sophisticated convolution-based signal model is proposed for simulation of stepped-frequency GPR images. This model takes into account the basic radar parameters (energy potential, frequency, antenna beamwidth, number of transmitted chirps, wideband of transmitted chirps and so on) and the basic parameters of a multi-layered medium (number of layers, dielectric properties of layers, depth of layers, attenuation) and, therefore, it results in more accurate simulation of stepped-frequency GPR images. The simulation results show that this algorithm can be successfully used for analysis and parameter optimization of the signal processing algorithms in stepped-frequency GPR.

1.3.1 Echo signal simulation

The synthetic high-resolution range profile is constructed by transmission of narrowband LFM pulses with frequency bands separated by a fixed step. At the m -th transmission of a narrowband LFM pulse, the signal reflected from a medium with L layers can be described as:

$$r(m, t) = r_0(m, t) + \sum_{k=1}^L \mu_{m,k} \sqrt{SNR_k} s(m, t) * \delta_k(m, t - \tau_k) + N_0(m, t) \quad (1.12)$$

where $r_0(m, t)$ is the direct normalized pulse from transmitting to receiving antennas; $s(m, t)$ -the transmitted LFM pulse whose envelope is unity; SNR_k is the signal-to-noise ratio from the interface between layers k and $(k + 1)$; $\mu_{m,k}$ - multiplicative noise; $\delta_k(m, t)$ - the impulse response of the interface between layers k and $(k + 1)$; τ_k - the two-way time delay of a signal reflected from the interface between layers k and $(k + 1)$; L -the number of layers; $N_0(m, t)$ is normalized Gaussian noise with zero mean and unity variation; and “ $*$ ” denotes convolution. Using the basic radar range equation and also taking into account the signal losses in the propagation path from the transmitter to the receiver, the SNR_k (in dB) can be evaluated as:

$$SNR_{k,dB} = \prod GPR_{dB} + \sigma_{k,dB} - 40lg\left(\sum_{j=1}^k z_k\right) - L_{k,dB}^{REF} - L_{k,dB}^{AT} - L_{R1,dB} - L_{R2,dB} \quad (1.13)$$

where $\prod GPR_{dB}$ is the radar energy potential (in dB); $\sigma_{k,dB}$ is the radar cross section of the interface between layers k and $(k + 1)$, z_k is the thickness of layer k ; $L_{k,dB}^{REF}$ is the signal loss due to signal reflections from the interface between two layers; $L_{k,dB}^{AT}$ is the attenuation loss; $L_{R1,dB}$ is the transmission loss from the antenna to the material; $L_{R2,dB}$ is the retransmission loss from the material to the air. Typically, for many earth materials, both $L_{R1,dB}$ and $L_{R2,dB}$ are about 2.5dB. The signal losses due to reflection of a signal from the interface between layers k and $(k + 1)$ are calculated as

$$L_{k,dB}^{REF} = -20lg\left(\Gamma_k \prod_{j=1}^{k-1} (T_{j,j+1} T_{j+1,j})\right) = -20lg(|\Gamma_k| \prod_{j=1}^{k-1} (1 - \Gamma_{j,j+1}^2)). \quad (1.14)$$

The reflection coefficient Γ_k and the transmission coefficient T_k in (14) are defined as:

$$\Gamma_k = (\sqrt{\varepsilon_{k+1}} - \sqrt{\varepsilon_k}) / (\sqrt{\varepsilon_{k+1}} + \sqrt{\varepsilon_k}); T_k = \sqrt{4\sqrt{\varepsilon_k \varepsilon_{k+1}} / [\sqrt{\varepsilon_{k+1}} + \sqrt{\varepsilon_k}]^2} \quad (1.15)$$

where ε_k is the permittivity of layer k . The attenuation loss of the material and the radar cross section are calculated as:

$$L_{k,dB}^{AT} = 4 \sum_{j=1}^k \alpha_j z_j \quad \text{and} \quad \sigma_k = \pi (\tan(\Theta/2) \sum_{j=1}^k z_j)^2 \quad (1.16)$$

where α_j is the attenuation constant in the j -th layer, and Θ is the beamwidth of the transmitter/receiver antenna.

1.3.2 GPR image simulation

The simulation algorithm for GPR images is shown in Figures 3 - 4. As can

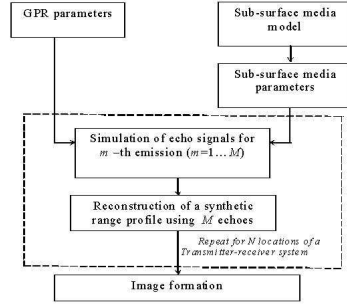


Fig. 1.3 Simulation of a range profile

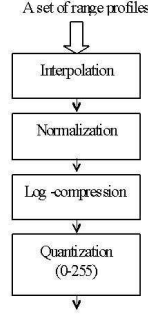


Fig. 1.4 GPR image formation

be seen, it includes two main stages: (1) - synthetic range profile formation. This procedure is repeated for each of N positions of a transmitter/receiver system. (2) -B-mode image formation. This procedure uses N synthetic range profiles obtained at a previous stage. According to Figure 3, simulation of M transmissions of LFM pulses results in the signal matrix of M columns, where each column contains the echo signal received after transmission of a LFM pulse. The simulated signal matrix is used for further construction of a synthetic range profile by one of the two methods, the time-domain method or the frequency-domain method [5]. According to Figure 4, the signal matrix with N columns, containing N synthetic range profiles, is used for GPR image formation. The stage of image formation includes such operations as interpolation, logarithmic-compression, quantization, and color visualization.

1.3.3 Simulation results

The simulation of B-mode images of a four-layered medium is done by using the convolution-based model described above. The simulated medium includes successive layers of dry sand, green sand, saturated sand and granite with depths of 31m, 21m, 16m and 24m, respectively. The electromagnetic parameters of layers (relative permittivity and attenuation) are $\epsilon = (4; 9; 15; 9)$ and $\alpha = (0.03; 0.1; 0.3; 0.2)$, respectively.

The following radar parameters are used for calculation of the SNR for each layer: radar energy potential - 120dB; antenna beamwidth - 20° ; pulse repetition frequency - 300 kHz; number of LFM pulses needed for construction of each synthetic range profile - 14, frequency bandwidth of a single LFM

pulse -2.4 MHz; total frequency bandwidth - $[4.6 \div 38.2]$ MHz; sampling frequency at RF -80 MHz; sampling frequency at baseband -2.5 MHz. The

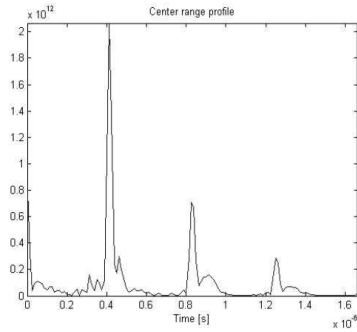


Fig. 1.5 The synthetic range profile

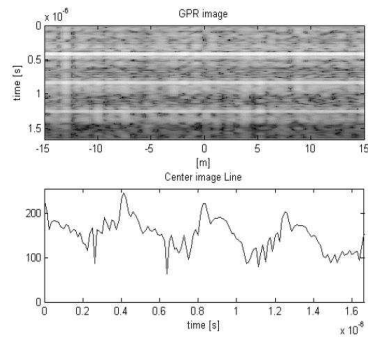


Fig. 1.6 Simulated B-mode image

SNR calculated for a signal reflected from layer 2 is 57 dB, from layer 3 - 40 dB and from layer 4 - 21dB. The corresponding two-way time delay of a signal reflected from layer 2 is 0.4 μ s, from layer 3 - 0.8 μ s, and from layer 4 - 1.25 μ s.

The time-domain stepped-frequency method is used to produce synthetic range profiles. The synthetic range profile, constructed in the time domain, and the simulated B-mode GPR image are shown in Figure 5 and in Figure 6 respectively.

1.4 GPR Data Basic Processing

The most important basic processing algorithms which are used in [10] have been developed earlier for GPR signal processing. The analysis of GPR data is carried out by processing the data using different filtering techniques and gains.

The most important basic processing algorithms in our case are:

- *Mean filter* (vertical working low-pass filter). This filter acts on each trace independently. The filter performs a mean over a selectable number of time samples for each time step;
- *Running average* (horizontal working low-pass filter). This filter acts on the chosen number of traces. The filter performs a running average over a selectable number of traces for each time step;
- *Stack traces* (compression in horizontal direction). This filter performs a temporal simultaneous stacking of a selectable number of traces.
- *Median filter* (pulse jamming and speckle noise reduction). This filter calculates the median over a selectable time/range area for each time step.

- *Background removal* (spatial high-pass filter which makes visible the shallow objects). This filter performs a subtracting of an averaged trace which is built up from the chosen time/distance range of the actual section.

- *Gain adjustment* (corrects the attenuation losses and makes visible the deep objects). The gain acts on each trace independently. The algorithm parameter (window length) forms a jumping window. The time window samples are normalized in range [0-1]. The experimental results obtained enable one to conclude that the algorithms for the basic signal processing presented in [10] can be successfully used for analysis of GPR images.

1.4.1 GPR Data Basic Processing- simulation results

In this section some results obtained by the above-mentioned algorithms are shown. The simulated image of a subsurface medium with five layers masked by pulse jamming is shown in Figure 7. It can be seen that after range profile formation, the pulse jamming looks like speckle noise. In order to remove this noise, a median filter can be applied over the selectable time/range area for each time step. In Figure 8, the real radargram acquired by the radar GSSI SIR is contaminated with pulse jamming (Figure 7). The same image “cleaned” by median filtering is shown in Figure 8. The image presents five underground fuel storage tanks. Benefits of the gain adjustment

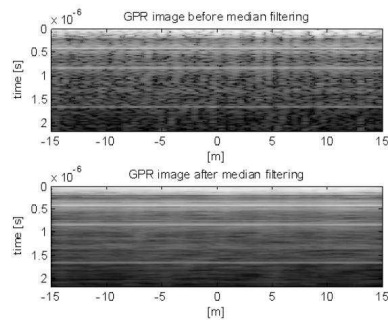


Fig. 1.7 Median filtering: nr. of time samples = 3; nr. of traces=21

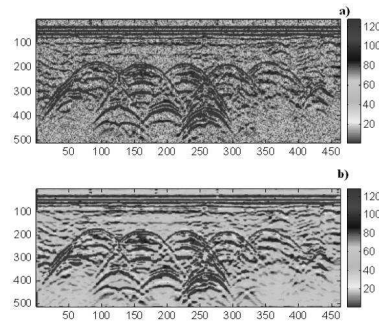


Fig. 1.8 Median filtering: nr. of time samples =5; nr. of traces = 5

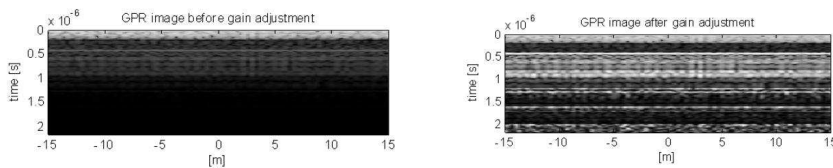


Fig. 1.9 Gain adjustment corrects the attenuation losses

algorithm are illustrated in Figure 9. The simulated radargram of a subsurface medium with five layers that is reconstructed in frequency is shown in Figure 9 (on the left). The gain adjustment applied to this image is also shown in Figure 9 (on the right). The gain acts on each trace independently. As a result, this algorithm makes the deep objects visible. The time window samples are normalized in range [0-1]. However this process destroys the original information of the signal. Therefore it is recommended to be applied only for displaying the GPR radargram.

1.5 CFAR filter approach for GPR processing

A conventional Constant False Alarm Rate (CFAR) detector is often used in primary radar signal processing and is very effective in case of stationary and homogeneous interference. Different approaches proposed in [7] are realized in different structures of CFAR detectors for operating in non-stationary non-homogeneous background and random impulse noise. One of them proposed by Rohling for a multi-target situation is to use the ordered statistics for estimation of the noise level in the reference window. Another approach is to excise high-power samples from the reference window before processing by the conventional cell averaging CFAR detector.

This approach is used by Goldman for design of an excision CFAR detector (EXC CFAR) in order to improve the performance of CFAR detectors in the presence of impulse interference.

It is obvious that two CFAR processors can be used as 2D filters of GPR images. The first of them visualizes images after adaptive thresholding (1 or 0), while the second filter visualizes only amplitudes above the adaptive threshold.

1.5.1 CFAR filters analysis

In modern radar, signal detection is declared if the signal value exceeds a preliminary determined adaptive threshold. The threshold is formed by current estimation of the noise level in the reference window. In this processor, the target is detected according to the following algorithm:

$$\begin{cases} H_1 : \Phi(q_0) = 1, q_0 \geq T_\alpha V \\ H_0 : \Phi(q_0) = 0, q_0 < T_\alpha V \end{cases} \quad (1.17)$$

where H_1 is the hypothesis that the test resolution cell contains echoes from the target and H_0 is the hypothesis that the test resolution cell contains

randomly arriving impulse interference only. $V = \sum_{i=1}^N x_i$ is the noise level estimate. The constant T_α is a scale coefficient, which is determined in order to maintain a given constant false alarm rate (CFAR).

The presence of randomly arriving impulse interference in both the test resolution cells and the reference cells can cause drastic degradation in the performance of such a CA CFAR processor.

To overcome the heavy noise environment where the detection is performed, a CFAR processor with Binary Integration (CFAR BI) is proposed. This signal processor can be considered as N single dimensional CA CFAR processors working in parallel. The binary integration processor employs a two-step thresholding technique for target detection. Firstly, a preliminary decision is made about each pulse of the pulse train reflected from a target. Pulse detection is declared if the first adaptive threshold is exceeded in the test cell. For this aim, the conventional CFAR detector can be used. Secondly, the number of samples, where the first threshold is exceeded, are counted and the obtained number of detections is compared with the second threshold. Target detection is declared if the second threshold is exceeded. The results in [7] show that the CFAR BI detector is more effective in conditions of intensive randomly arriving impulse interference.

CFAR processors with post detection integrators are proposed for the case of a homogeneous environment and chi-squared family of target models (CFAR PI). The possibility for parallel processing of samples in the reference window can be realized by a parallel computing architecture of the target detection algorithm. This post detection integration (PI) CFAR processor consists of a single pulse matched filter, square-law envelope detector, linear post detection integrator, noise level estimator and comparator.

1.5.2 CFAR filters - simulation results

One real GPR image containing a waste water pipe and a land mine under a thin layer of wet sand is presented in Figure 10. Three images after the CA CFAR filtering are shown on Figures 11-13. They are performed by a 16-element moving window in depth and scale constants $T = 1, 1.1, 1.3$. When the scale factor increases the borders between layers become less visible. For higher values of T the presence of foreign substances (land mines, pipes) is more perceptible. When CFAR PI filtration is applied to the image from Figure 10, the result in Figure 14 is obtained. The performance is done with a rectangular window of size (16X16) and $T = 18$.

After CA CFAR BI processing of the image from Figure 10, the result is shown on Figure 15. The binary integration with rule 10/16 leads to the results depicted on Figure 15. In this case the reference window is of size (16X16) and $T = 6$.

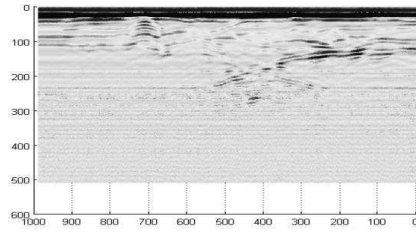


Fig. 1.10 Geo-radar profile (waste water pipe and a land mine)

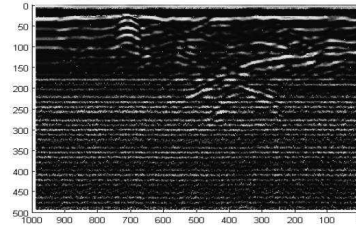


Fig. 1.11 Geo-radar profile after CA CFAR filtering ($T=1$)

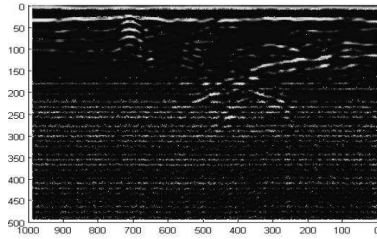


Fig. 1.12 Geo-radar profile after CA CFAR filtering ($T=1.1$)

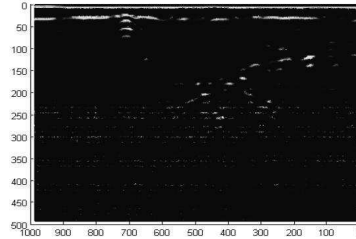


Fig. 1.13 Geo-radar profile after CA CFAR filtering ($T=1.3$)

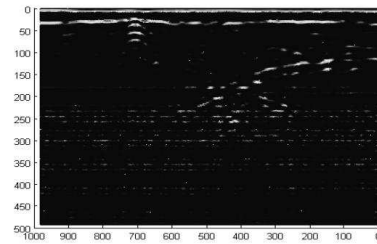


Fig. 1.14 Geo-radar profile after CFAR PI filtering ($N = 16, M = 16, T = 18$)

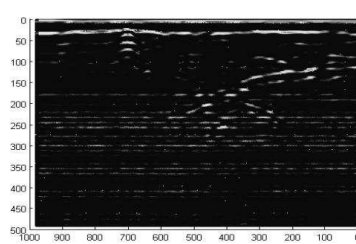


Fig. 1.15 Geo-radar profile after CFAR BI processing with binary rule 10/16)

1.6 Hough approach in GPR processing

The Hough Transform (HT) is regarded as a template matching method for feature detection. The conventional HT approach is usually used for straight line detection and linear objects localization. However, the HT can be successfully used for ellipse or circle detection and even for arbitrary form detection. As a consequence, the HT algorithm can be applied to buried mines detection transforming all image pixels by automatic detection of circular shapes [1].

1.6.1 Hough transform based hyperbola detection

The standard hyperbola equation doesn't meet all GPR constraints. To deal with the antenna speed fluctuation and the anisotropic wave propagation an additional parameter is included in this equation. The slightly modified equation takes the form:

$$y(t_i) = \sqrt{k^2(x_r(t_i) - x_0)^2 + d_{min}^2}. \quad (1.18)$$

A parameter k may express the difference between the antenna speed and the basic speed ν_{0x} :

$$y(t_i) = \sqrt{\left[\frac{k(x_r(t_i) - x_0)}{t_i - t_k}(t_i - t_k)\right]^2 + d_{min}^2} = \sqrt{[k\nu_{0x}(t_i - t_k)]^2 + d_{min}^2}. \quad (1.19)$$

k may also express the variations of the velocity of wave propagation when spreading through the subsurface medium:

$$\begin{aligned} y(t_i) &= \sqrt{k^2(x_r(t_i) - x_0)^2 + d_{min}^2} = k\sqrt{(x_r(t_i) - x_0)^2 + \left(\frac{d_{min}}{k}\right)^2} = \\ &= k\sqrt{(x_r(t_i) - x_0)^2 + D_{min}^2} = k\nu_{0x}(t_i - t_k) \end{aligned}$$

where ν_{0x} is the accepted wave propagation velocity through the earth.

There are two approaches for hyperbola maximum localization by HT. The *first* considers two consecutive standard (for straight line detection) HTs, followed by a logical analysis of detection of the corresponding lines. The idea is to approximate a hyperbola with two straight lines (Figure 16) and find them with the standard HT. These straight lines have the restricted space position (depending on the parameter variation), and the algorithm requires limited computer resources. The main drawback is that the accumulator doesn't contain information about coordinates of points. As a result many hyperbolas will be detected, but most of them will be false. A complex combinatorial algorithm has to be applied to reject ghost hyperbolas. The second drawback concerns the horizontal hyperbola's part. This part is usually formed by the most powerful echoes from the target of interest with the highest signal-to-noise ratio. That is the main reason to regard this part as the most reliable source of information about the target position. But in the first approach it isn't considered at all.

The *second approach* applies the HT directly to equation (19). In this case the HT uses 3D parameter space. The three parameters are x_0, y_0, k . The larger parameter space presumes more time for searching the peak and requires more memory. Still the second approach is accepted as a more perspective one. The hyperbola strip width is matched to errors, generated by the antenna speed fluctuation and by the variable velocity of propagation. The hyperbola strip is convolved with a Gaussian filter to weight the votes, falling from points, lying on the central (for this strip) hyperbola, and the votes from points lying aside it (Figure 16).

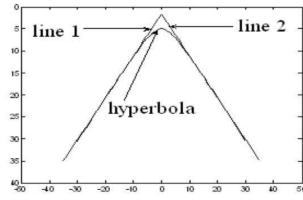


Fig. 1.16 Hyperbola approximation with two straight lines on hyperbola

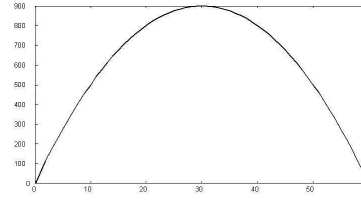


Fig. 1.17 Nonlinear asymmetrical weighting (for the case of 60 received votes)

1.6.2 Algorithm realization and simulation results

The generalized HT algorithm requires transformation of each image point from the image (feature) space to the parameter space and accumulates their votes. Usually the GPR images include not less than 0.5M pixels, every pixel with 216 or 28 intensity levels. The problem is to find such pixels of similar intensity lying on a hyperbola (or near to it) that differ from the neighboring pixels. It is obvious that the computer processing of a whole set of image points is a tedious task, requiring serious computer resources. This problem is solvable, but the algorithm will be intensity dependent, which is an undesired characteristic of every image processing algorithm. To reduce the initial set of potential points belonging to hyperbolas, filtering algorithms are applied. Real-time solution of the task includes several steps: the GPR input; 2D FFT filtering; Canny edge detection; HT hyperbola detection; visualization.

The strongest and almost constant echo-signals are received from borders between different subsurface layers (Figure 18a). These echo-signals play a role as powerful low frequency noise and should be removed from the image. The high frequency noise is also present in the image and looks like one or a few grouped pixels in the image, strongly differentiating from the surrounding pixels. To reject them a 2-D band-pass frequency filtering is applied over a raw GPR image. The lowest and the highest several frequencies are rejected, including the constant or DC Fourier component. The filter band-pass frequencies are matched to both the antenna speed and the echo-signal attenuation. The band-pass frequency filtering is realized in three steps: 1) Fast Fourier Transform (FFT); 2) Weighing the Fourier components; 3) Inverse FFT. The image may be preprocessed in order to limit the bandwidth. For example, Gaussian smoothing can be applied in advance.

For GPR data, the most suitable Fourier components of a 2-D frequency filter are chosen as follows: For the highest frequencies, the last 5 Fourier components in both directions, horizontal and vertical, are nulled. For the lowest frequencies, the first 30 Fourier components in the horizontal direction are nulled and the first 10 components in the vertical direction are nulled (rectangular window). Using frequency domain filtering, excellent robustness

against correlated and frequency dependent noise is achieved (Figure 18b). Careful analysis of the output image shows an appearance of weak Gipp's effects near the image borders, but without the influence on the edge detection algorithm.

The Canny edge detector is used as an image contour detection algorithm. The Canny method finds edges by looking for local maxima of the gradient of the pixel intensity. The gradient is calculated using the derivative of a Gaussian filter. The method uses two thresholds for detecting the strong and the weak edges, and includes the weak edges in the output only if they are connected with strong edges. This method is therefore less sensitive to noise than the others, and it can localize true weak edges. The Canny edge detector is used mainly to reduce the number of pixels of interest by two orders of magnitude. The final result is very promising - the number of non-zero pixels in GPR images is reduced from 0.5M to several thousands. The values of chosen parameters are: 0.3 - for lower threshold, 0.33 - for higher threshold and 3 - for standard deviation of the Gaussian filter (Figure 18c).

The HT algorithm is realized as follows. Two windows, one for the left half of a hyperbola and the second for the right half of a hyperbola are generated. Both windows are applied to the image at the output of a Canny edge detector. As a result, two accumulator spaces are obtained for the left and the right half of the hyperbola. How to merge them? This step is very important for the final result of the whole filtering. Practice proves that robust results are obtained only if there is symmetry of votes for both parts. The

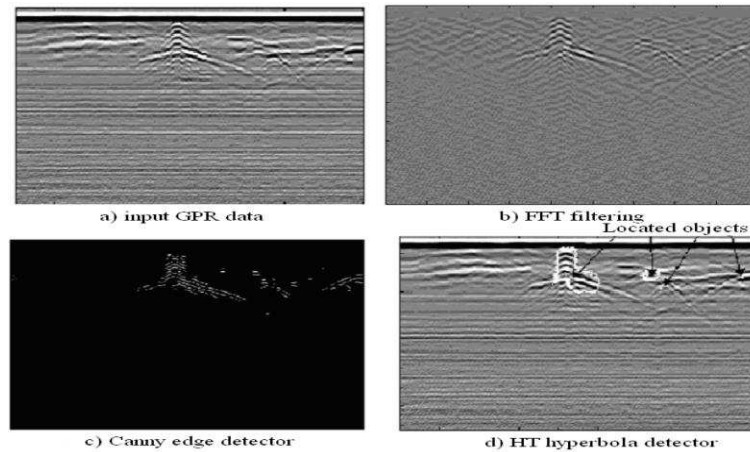


Fig. 1.18

proposed algorithm realizes the common accumulator space by multiplication of contents of both accumulator spaces, element by element. It is clear that this operation will amplify accumulators in both parameter spaces with the equivalent number of votes and will weaken accumulators with asymmetric distribution but with the equivalent sum of votes to the previous case

in both parameter spaces (Figure 18b). Peak detection is performed after thresholding. The located objects are displayed on Figure 18d.

1.7 A Bayesian algorithm for object detection in GPR data

A number of sophisticated techniques for background signal reduction and object detection have been proposed, accounting for the nonstationary and correlated nature of GPR signals. They usually incorporate complex models and time-consuming learning stages for model parameter adjustment. The aim of this investigation is to use simple models with robust processing algorithms.

A GPR data processing algorithm relying on simple background and target models is suggested by Dr. Carevic, cited in [3]. It is based on the “variable dimension filtering approach” to target tracking. Background estimation, target detection and target-background separation are performed within a common Kalman filter-based computational procedure. This algorithm is successfully applied to reduce the background interference signals and to detect shallow buried targets. However, in the case of large state dimensions the target signal estimate can be unsatisfactory. Also, additional information is needed for identifying target extent.

The novelty of the results obtained in [2, 3] is that the constructive elements of a Kalman filtering approach are extended with the advantages of hybrid Bayesian estimation. The set of GPR data is processed in two consecutive steps. At the first step, a part of the algorithm of Dr. Carevic is realized: a Kalman filter (KF) estimates the background signal, time-varying noise characteristics and detects possible targets. The estimated noise parameters are utilized at the second step, where an Interacting Multiple Model (IMM) algorithm is applied. Using multiple models and efficient Bayesian mechanism for information fusion, the IMM algorithm assesses more precisely the target signal and target extent. The IMM posterior model probabilities assist in the decisions of the Kalman filtering procedure, increasing the probability of target detection.

Change detection methodology provides efficient tools for automatic on-line (or off-line) signal segmentation. The cumulative sum (CUSUM) tests are computationally simple and robust procedures, giving relevant results in the cases of slowly time-varying signals before and after the abrupt change. A sequential CUSUM test is developed and investigated using the innovation properties of the Kalman filter as the next stage of the target recognition system. The experiments show promising results in terms of estimation accuracy, probability of target detection and false alarm probability [3].

1.7.1 Processing algorithms

B-scan (or radargram) data contain the received GPR signals $u(n, k)$, where $n = 0, \dots, N - 1$ denotes the signal time samples and $k = 0, 1, \dots$, corresponds to the spatial position of the receive antenna. In the framework of state space representation, the radargram data are divided into P non-overlapping horizontal strips with depth m . Based on appropriate models, a set of P KFs is run in parallel on each data strip. Next, a set of P IMM filters is implemented, using the KFs' output parameters. The estimators work independently of each other, but exchange information for more reliable decision making. The goal of this combined KF-IMM algorithm is to detect and estimate target signals by fragmenting the data into target and background regions. The algorithm can be summarized by the following two steps.

Step I: A KF for background estimation and target detection. Using a “quiescent state model” [3] and the GPR measurements, the KF recursively produces a background state estimate with its associated state covariance. The properties of measurement residual (innovation) are employed to detect the targets and to adapt the filter to time-varying background parameters. The detection algorithm uses a χ^2 test and innovation-based statistic (normalized innovation squared (NIS) [3]) to detect the presence of possible targets. Under the hypothesis that the target is not present (“target-free” hypothesis), the NIS has a χ^2 distribution with m degrees of freedom. If NIS exceeds a threshold, determined by some level of significance, a procedure for target detection is initiated. If the “target-free” hypothesis is rejected for at least K_1 consecutive spatial positions (traces) and for at least K_2 of the total of P strips, the target is considered to be detected and its size is determined proportionally to the values of K_1 and K_2 .

Noise identification. The correct knowledge of process and measurement noise statistics is a prerequisite for consistent KF operation. In general, the noise statistics are not known or partially known. The measurement error covariance can be estimated on line or selected a priori according to some rules or practical considerations. In the present realization it is determined through the variances of the radargram data, calculated along the traces for each strip. Due to soil inhomogeneities, the background signal slowly varies with trace numbers k and soil layers $p = 0, 1, \dots, P$. The filters are adapted to this feature by using time-varying process noise characteristics. Two background adaptation procedures are implemented and experimented here. According to the first one, the noise covariance is updated recursively by a scaling factor. At each trace number k , the scaling factor is modified according to logic, managed by the NIS values and a set of thresholds, selected according to χ^2 distribution. A hybrid estimation technique for noise identification is also realized and experimented.

Step II: An IMM filter for target signal estimation and target-background separation. Using multiple models, accounting for different data regions (background or background plus target), the IMM algorithm has a poten-

tial for robust data segmentation. The IMM design configuration incorporates three models. The first one corresponds to the hypothesis that only a background is present. The process noise covariance is obtained by the background adaptation procedure, implemented at Step I. The target is modeled approximately as a stochastic bias with different magnitudes. The next two models match to the hypotheses that a bias is available in addition to the background. The input noise covariances are selected in such a way that the signal jumps caused by the targets can be detected and estimated. The IMM filter produces a combined state estimate as a weighted sum of model-matched estimates. The posterior model probabilities segment the radargram data into target and no-target areas. Comparison with the KF detection output can help for more reliable target identification.

A great variety of change detection tests are proposed and investigated in the statistical literature. Here, the CUSUM test is appended to the KF algorithm (discussed in Step I) in order to increase the probability of target detection.

A Kalman filter with CUSUM test for B-scan data segmentation. It is found in the investigations devoted to GPR data processing, that the residual energy obtained by removing background components from the GPR signal is more reliable for change detection. Based on this inference, we apply the CUSUM algorithm to the difference between the radargram data and background state estimate. If the evolution of this subtracted signal is described by a simplified linear model, a KF can be implemented to yield the subtracted signal state estimate. If the target is not present, the measurement residual is zero mean, Gaussian and white. The signal anomalies, caused by the objects, alter the parameters of the Gaussian distribution. Thus, the task of target onset detection is transformed to the problem of change detection in the Gaussian distribution. Practically, the change point detection is approximately considered as the detection of changes in the mean value of the Gaussian distribution. A simple recursive two-sided CUSUM test is realized and experimented. It confirms the decisions of the KF-based detector and provides additional information for target onset. The CUSUM test is also applied to the transposed GPR image. Thus, the test approximately outlines the borders between the layers and can be used for the purposes of ground layers segmentation.

1.7.2 Experimental results

Algorithm performance is studied over a series of real radargrams, acquired by GSSI SIR Systems. The design parameters are chosen as follows: the depth of the horizontal strips is $m = 50$ and the number of strips is $P = 6$. The parameters of the KF detection algorithm are selected as follows: $K_1 = 15$ and $K_2 = 2$. The combined KF-IMM algorithm detects two objects in the image,

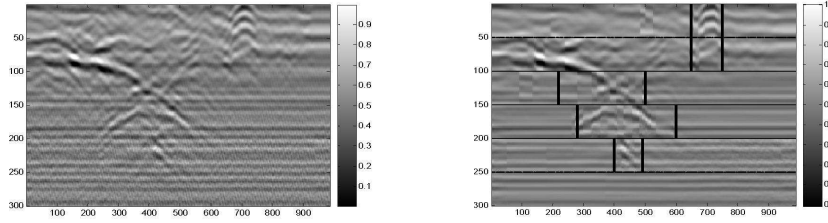


Fig. 1.19 a) Original GPR image and b) estimated objects' position by KF-IMM

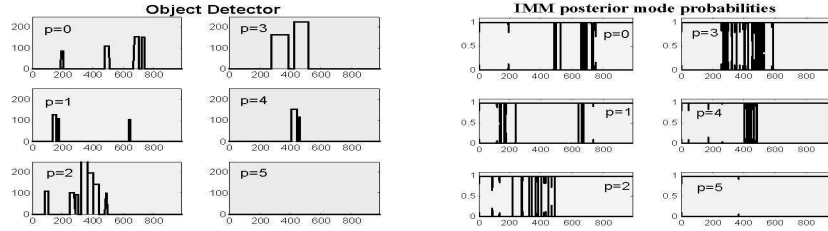


Fig. 1.20 a) KF object detector and b) IMM detector by KF-IMM

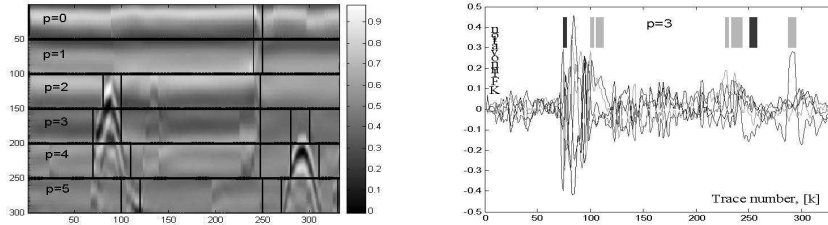


Fig. 1.21 a) KF-IMM algorithm detects two pipes b) CUSUM detector confirms the KF results at $p = 3$

presented in Figure 19a. Outputs of the KF and IMM detectors are presented in Figure 20a and Figure 20b, respectively. Based on this information, the objects' positions are approximately determined, as can be seen in Figure 19b. The first object (a sewerage pipe under consideration) is positioned over 3 consecutive layers ($p = 2, 3, 4$) and its presence is confirmed by both detectors. Since the second object (positioned on strips $p = 0, 1$) is a clutter object, additional information about the pipe size is needed to discard it. The KF-IMM algorithm detects two real objects in the image presented in Figure 21a. The CUSUM test, implemented after the KF procedure, validates the presence of the objects (Figure 21b).

1.7.3 Implementation of Low-Frequency GPR Signal Algorithms using a conventional narrowband digital transmit-receiver systems

The earlier described stepped-frequency approach with time domain reconstruction reveals a possibility to obtain high-range resolution images with a conventional narrow-band transmitter/receiver digital system for GPR implementation. A survey was performed to test the maximal frequency bandwidth by using a traditional narrow-band transmit/receiver system composed of commercial signal processing devices: ADC(AD6644), DAC(AD9772), receiver, synthesizer, on-line signal processor running on a PC. In that way the whole ADSs and DACs bandwidth (60 - 100 MHz) can be filled up with a set of narrow-band Receiver/Tranceiver Signal Processors (RSP AD6624 and TSP AD6623 - 2.2MHz) [4]. A multi-module and a multi-channel digital system composed of narrowband receivers (RSPs) and transmitters (TSPs) (Figures 22, 23) is developed in order to transmit and receive wideband signals within the whole frequency band of commercial ADCs and DACs. It is a traditional hardware approach, which unfortunately requires multiple control of a multi-module digital system and, evidently, involves high financial expenses [4]. Considering the limitation parameters of the Signal Processors (RSP AD6624 and TSP AD6623), a Monte-Carlo approach for their parameter optimization is used. Only four parameter sets of the stepped frequency processing are found for the implementation in GPR. The theoretical calculations show that the role of a GPR stepped-frequency algorithm in the time domain, quadrature demodulation and decimation, can be implemented on the basis of a single 4-channel Analog Devices's AD6624 and AD6623 using at most two channels [4]. Figure 24 shows the MPS signal processor based on two DSP signal processors and conventional industrial box, which encapsulates the signal processing hardware and is used in MPS Ltd. for a GPR system.

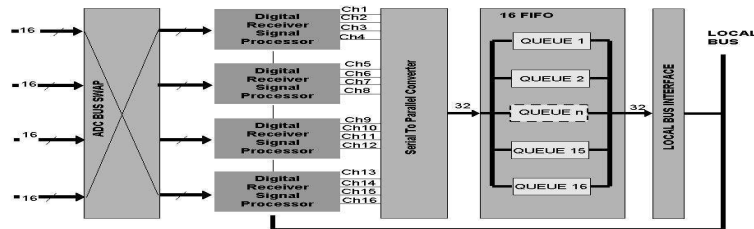


Fig. 1.22 Block diagram of the digital receiving system based on four-channel receive signal processors (RSP) AD6624

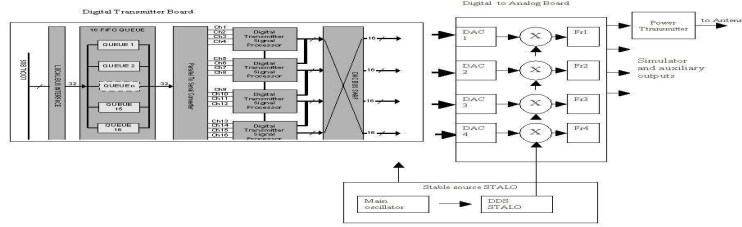


Fig. 1.23 Block diagram of the digital transmitting system based four-channel transmit signal processors (RSP) AD662

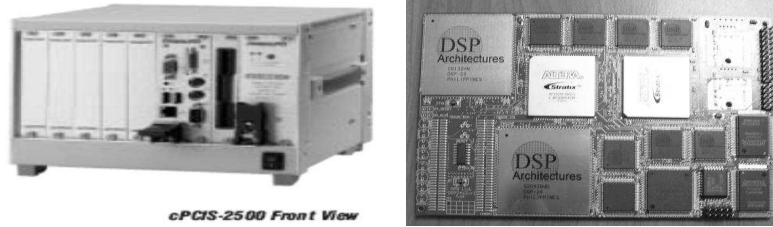


Fig. 1.24 The conventional industrial box, which encapsulates the signal processing hardware in a MPS Ltd. GPR system and the signal processor based on two DSP signal processors

1.7.4 FPGA Implementation of a Low-Frequency GPR signal algorithm

This paragraph reveals a possibility for implementation of the stepped-frequency algorithm with time-domain reconstruction on a hardware platform in real time i- a step closer to real implementation. The hardware reconfigurable platform XUPV2P, based on VIRTEX II Pro technology is used (Figure 26). A block diagram of the algorithm suitable for a reconfigurable hardware implementation is presented in Figure 25. All computational kernels from the algorithm are designed as separate hardware blocks, and verified individually and stacked together. Considering the previously described stepped frequency algorithm [5], a block diagram of the receiver was made. It consists of: down conversion; interpolation; phase correction; frequency shifting; buffering the whole constructed signal; correlation; envelope detection, normalization and image storing. The block diagram of the receiver is shown in Figure 25. The number of transmitted pulses is $M = 14$. The sampling frequency of the signal is 80Mhz, the sampling frequency of the video signal - 2,25Mhz, minimal frequency carrier $f_{min} = 4.6Mhz$, maximal frequency carrier $f_{max} = 38.2Mhz$, the step in frequency is $d_f = 2.4Mhz$. The frequency sweep rate is $b = \Delta f / Tp$. Tp is the time duration of a narrow-band chirp, in our case - 1.6ms. The down converter is implemented according to the specifications of the Digital Down Converter (DDC) V1.0 (Xilinx IPTM) [9]. It encompasses the following processing: Quadrature Amplitude Demodula-

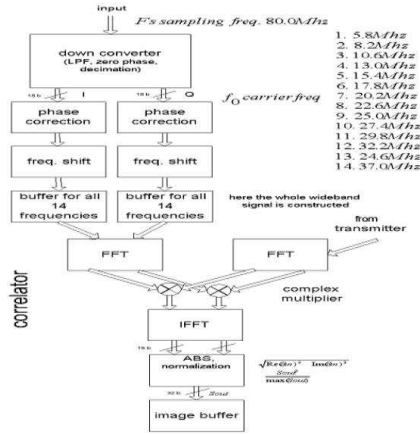


Fig. 1.25 Block diagram of the receiving structure)

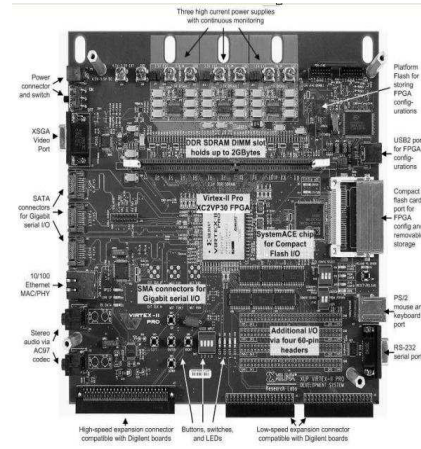


Fig. 1.26 XUP™ Virtex-II Pro Development System

tion, Low Pass Filter and decimation by 32. The input signal consists of 5376 samples. The tests were performed considering following parameters: System frequency rate: 100Hz; Input signal frequency: 80MHz; Input data width: 16 bits; Output data width: B8=18 bits; Spurious dynamic range of the digital synthesizer: 40dB; Frequency resolution: 0.5MHz; Phase angle: fixed; Output mixer width: 20 bits. The finite impulse response (FIR) filter is included in the synthesis of the digital down converter, the decimation rate is 16; the FIR filter length is 16 and the result precision is 12. The time domain reconstruction follows. It consists of phase correction and frequency shifting. Next a buffer for signal reconstruction (coherent summing) follows. It consists of a standard storage buffer based on memory block core [2]. Considering the signal processing principles the correlator consists of multiplication between received and transmitted signals in the frequency domain. Therefore we put two 64-point FFT transforms, one each for the received signal and for the transmitted signal. Next an IFFT is needed to come back to the time domain (Figure 25) [8]. An envelope detector and a signal normalization follow (Figure 25). The envelope detector consists of two multipliers and a sqrt block, which is based on the CORDIC v.3.0 architecture [9]. The transceiver consists of a look-up table, which contains the signals for transmitting. The number of signals is 14 and each of them consists of 128 samples. The transmitted signal is formed by the Tukey window before sending it to the Digital to Analogue Converter.

Simulation results. The simulation results are obtained via the *Modelsim™* simulator [9]. A VHDL code was written, and studied through the *Modelsim™* simulator. After the performed simulation, the constraints for real time imaging were defined. The correlation is performed for 108 μ s. The total synthesis

estimation parameters are: number of slices = 8937; BRAM = 30; Mult18x18 = 62. After the simulation performing the real time constraints took approximately 400 μ s. According to the synthesis report, the usage of the processor was almost 75%.

1.8 Conclusions

The simulation results based on the Monte-Carlo approach enable us to conclude:

- The stepped-frequency GPR processing method for range profile formation in the time domain, operating at 4.6 MHz to 38.2 MHz, generates synthetic range profiles with the resolution of 1-2 m by transmitting 14 narrowband chirps at each GPR position.
- A new convolution-based algorithm for simulation of stepped-frequency GPR images from multi-layered media can be successfully used for analysis and parameter optimization in stepped-frequency GPR.
- The basic algorithms for GPR signal and image processing such as mean filters (vertical working low-pass filter), running averages (horizontal working low-pass filter), stack traces (compression in horizontal direction); median filters (pulse jamming and speckle noise reduction), background removals (spatial high-pass filter) that make visible the shallow objects and gain adjustment algorithms (correct the attenuation losses and make visible the deep objects) are effective algorithms for GPR image processing.
- Applying CFAR filters and Hough filters to GPR image processing is a good decision.
- The designed multiple models Particle Filter (PF) for contour determination and segmentation in GPR images has shown encouraging results in terms of convergence and accuracy, at the cost of acceptable computational complexity.
- Applying Kalman filters to GPR data processing gives promising results in terms of estimation accuracy, probability of target detection and false alarm.
- The processor VIRTEX II Pro is suitable for implementation of the stepped-frequency processing algorithm for synthetic range profiling in the time domain.

Generally speaking, the approaches and algorithms considered in this chapter can be successfully used for UXO signal processing and multi-sensor (channel) UXO signal processing.

References

1. Alexiev K., "Object Localization in Ground Penetrating Radar Images", *Comptes rendus de l'Academie Bulgare des Sciences*, Tome 60, No 11, 2007, pp. 1237-1244 .
2. Angelova D., P. Konstantinova, L. Mihaylova, "Contour Tracking in 2D Images Using Particle Filtering", *Proc. of the IRS'2007*, 5-7 September, Cologne, Germany, pp. 515-519.
3. Angelova D., "A Bayesian Algorithm for Object Detection in GPR Data", *Proc. of the IRS'2008*, 19-23 May, Wroclaw, Poland, pp. 301-304.
4. Babalov S., V. Vassilev, P. Daskalov, Chr. Kabakchiev, "DPCR-Development Platform for Digital Communications and Radars", *Proc. of the IRS'2004*, Warsaw, Poland, pp. 131-136.
5. Behar V, Chr. Kabakchiev, "Stepped-Frequency Processing in Low Frequency GPR", *Proc. of the IRS'2007*, 5-7 September, Cologne, Germany, pp. 635-639.
6. Behar V, Chr. Kabakchiev, "A Simple Algorithm for Simulation of Stepped-Frequency GPR Images of Multi-Layered Media", *Proc. of the IRS'2008*, 19-23 May, Wroclaw, Poland, pp. 289-292.
7. Garvanov I., V. Behar, Chr. Kabakchiev, "CFAR Processors in Pulse Jamming", *Proc. of Conference "Numerical Methods and Applications" - NMA02*, Borovets, Bulgaria, LNCS 2542, 2003, pp. 291-299.
8. Daniels D., *Ground penetrating radar*, 2nd edition, The Institution of Electrical Engineers, London, 2004.
9. Kyovtorov V., Chr. Kabakchiev, V. Behar, G. Kuzmanov, I. Garvanov, L. Doukovska, "FPGA Implementation of Low-Frequency GPR signal algorithm using Frequency Stepped Chirp Signals in the time domain" *Proc. of the IRS'2008*, 19-23 May, Wroclaw, Poland, pp. 297-300.
10. Vassileva B., Chr. Kabakchiev, "Singular Spectrum Analysis (SSA) for GPR Data Processing", *Proc. of the IRS'2008*, 19-23 May, Wroclaw, Poland, pp. 293-296.